Compact Millimeter-Wave Circularly Polarized Filtering Antenna Using SIGW Technology

Chao Chen, *Member, IEEE*, Jianlin Han, *Student Member, IEEE*, Haoming Liu, *Student Member, IEEE*, Jun Wang, *Member, IEEE*, Ruofeng Xu, *Member, IEEE*, Lei Zhao, *Senior Member, IEEE*, Jixin Chen, *Member, IEEE*, and Ying Liu, *Fellow, IEEE*

***Abstract*—In this letter, a circularly polarized (CP) filtering grid-slotted patch antenna (GSPA) is proposed for millimeter-wave (MMW) applications. The antenna mainly consists of a corner-truncated patch radiator, a coupling slot, and a substrate-integrated gap waveguide (SIGW) feeding network. By properly incorporating several parasitic structures, the proposed design achieves wide axial-ratio bandwidth (ARBW) and good stopband suppression. Specifically, a cross strip and four parasitic strips are introduced to broaden the ARBW, while the radiator, coupling slot, and feeding network together form a third-order filter for upper stopband suppression. In addition, a circular ring and two folded strips are incorporated to generate two radiation nulls in the lower stopband. Since the added parasitic structures occupy no additional space, the antenna remains compact with an aperture of only $0.37\lambda_0 \times 0.37\lambda_0$. For validation, a 1 × 4 filtering antenna array is fabricated. Measurements show a −10 dB impedance bandwidth (IBW) of 23.3% and a 3 dB ARBW of 27.8%, fully covering the 5G MMW band (24.25–29.5 GHz). Meanwhile, the out-of-band suppression is greater than 22 dB.**

***Index Terms*—Compact, circularly polarized (CP), filtering antenna, millimeter-wave (MMW), substrate-integrated gap waveguide (SIGW).**

I. Introduction

With the rapid advancement of fifth-generation (5G) mobile communications, the millimeter-wave (MMW) frequency band has emerged as a crucial spectral resource for achieving high data rates [1], [2]. To reduce the size of MMW radio-frequency (RF) front-ends, a design concept of filtering antennas has been proposed [3]-[8]. Based on existing reports, the design approaches of filtering antennas can generally be categorized into two types.

The first category is the synthesis approach [3]-[5]. Undoubtedly, these filtering antennas provide excellent out-of-band suppression; however, integrating multiple resonators into the feeding network inevitably increases insertion loss. To address this issue, the fusion method has been proposed [6]-[8]. Since these designs do not require additional filtering circuitry, they feature a more compact size. Nevertheless, most of these designs operate in the sub-6-GHz band and support only linearly polarized (LP) radiation. To further address the above issues, several MMW circularly polarized (CP) filtering antennas have been proposed [9]-[11]. However, their impedance bandwidth (IBW) or axial-ratio bandwidth (ARBW) remains relatively narrow, failing to fully cover the 5G MMW band (24.25–29.5 GHz). Therefore, realizing a circularly polarized (CP) filtering antenna with wide IBW and ARBW still involves some technical challenges.

Grid-slotted patch antennas (GSPAs) have been widely used in communication systems due to their wider IBW compared with conventional patch and slot antennas [12], [13]. In recent years, the GSPA has been further developed to realize filtering functionality [14], [15]. However, most of these designs are LP and have relatively large apertures exceeding $0.77\lambda_0 \times 0.77\lambda_0$, where λ_0 is the free-space wavelength at the center frequency. For MMW antenna array systems, maintaining the radiation aperture of each antenna element below $0.5\lambda_0 \times 0.5\lambda_0$ is essential [16]–[18]. In this context, few compact filtering GSPAs have been proposed; however, they only achieve LP radiation [19], [20]. Thus, the design of a compact CP filtering GSPA is of considerable research interest.

The substrate-integrated gap waveguide (SIGW) feeding network offers lower transmission loss than the microstrip feeding structure owing to its self-packaged nature [21]. As a result, it has been widely adopted in various MMW filtering antenna array designs [22]–[24]. However, among these filtering antennas, only the design reported in [24] achieves CP radiation. Nevertheless, its 3-dB ARBW is only about 10%, which is insufficient to fully cover the entire 5G MMW band. Therefore, a SIGW-based CP filtering antenna with wide ARBW is highly desirable.

In this paper, a MMW CP filtering GSPA based on a SIGW technology is presented. This is, to our knowledge, the first CP

This work was supported in part by the Postdoctoral Fellowship Program of CPSF under Grant GZC20241929, in part by the Project of National Key Laboratory of Radar Detection and Sensing under Grant 2401074240307, in part by the Open Project of State Key Laboratory of Millimeter Waves under Grant K202527, and in part by the Fundamental Research Funds for the Central Universities under Grant 2025QN1060. (*Corresponding author*: Lei Zhao.)

Chao Chen is with the School of Information and Control Engineering, China University of Mining and Technology, Xuzhou 221116, China, also with the National Key Laboratory of Radar Detection and Sensing, Xidian University, Xi'an 710071, China, and also with the State Key Laboratory of Millimeter Waves, School of Information Science and Engineering, Southeast University, Nanjing 211189, China (e-mail: chaochen@cumt.edu.cn).

Jianlin Han, Haoming Liu, Jun Wang, Ruofeng Xu, and Lei Zhao are with the School of Information and Control Engineering, China University of Mining and Technology, Xuzhou 221116, China. (e-mail: jianlinhan@cumt.edu.cn; haomingliu@cumt.edu.cn; jun-wang@cumt.edu.cn; xuruofeng@cumt.edu.cn; leizhao@cumt.edu.cn).

Jixin Chen is with the State Key Laboratory of Millimeter Waves, Southeast University, Nanjing 211189, China (e-mail: jxchen@seu.edu.cn).

Ying Liu is with the National Key Laboratory of Radar Detection and Sensing, Xidian University, Xi'an 710071, China (e-mail: liuying@mail.xidian.edu.cn).

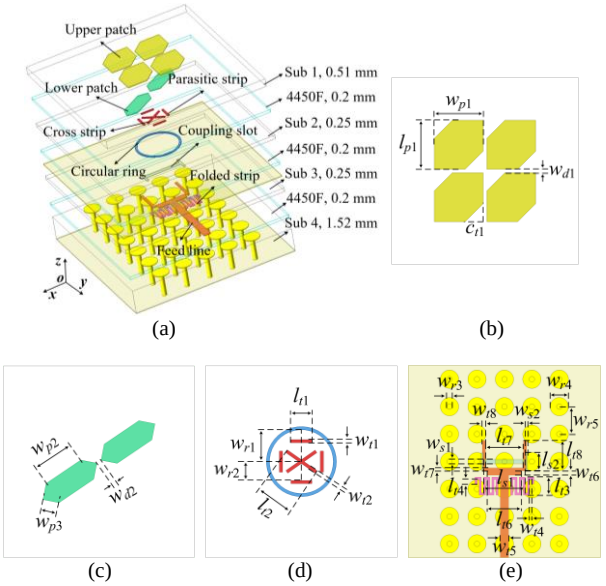

Fig. 1. Configuration of the proposed CP filtering antenna element. (a) Exploded view. (b) Upper patch antenna (top view). (c) Lower patch antenna (bottom view). (d) Sub 2 (top view). (e) Subs 3 and 4 (top view).

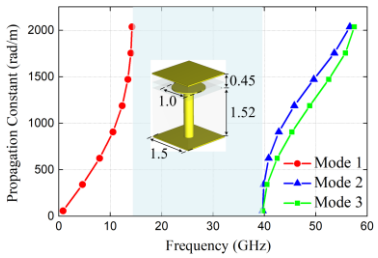

Fig. 2. Dispersion diagram of the EBG unit cell. (Dimensions are in mm.)

filtering GSPA with IBW and ARBW fully covering the 5G MMW band. Besides, the design features a compact structure with an aperture size of only $0.37\lambda_0 \times 0.37\lambda_0$. For validation, a prototype antenna is fabricated and measured.

II. Structure and Mechanism of the Proposed CP Filtering Antenna

A. Antenna Configuration

Fig. 1 illustrates the geometry of the proposed CP filtering GSPA. As shown in Fig. 1(a), the antenna unit mainly consists of four dielectric layers and three adhesive layers. From top to bottom, the four dielectric layers, designated as Sub 1 to Sub 4, are all made of Rogers 3003 (ε_r = 3 and tanδ = 0.0013), with thicknesses of h_1 = 0.51 mm, h_2 = 0.25 mm, h_3 = 0.25 mm, and h_4 = 1.52 mm, respectively. Furthermore, all adhesive layers are made of Rogers 4450F (ε_r = 3.52 and tanδ = 0.004) with a uniform thickness of 0.2 mm. Since the detailed design procedure of the SIGW feeding network is available in [25], it is omitted here for brevity. Fig. 2 presents the dispersion diagram of the final optimized electromagnetic bandgap (EBG) structure, whose stopband extends from 14.5 to 39.5 GHz. The relatively wide EBG stopband is intentionally adopted to suppress higher-order modes in the filtering antenna stopband, thereby avoiding degradation of its out-of-band suppression performance. The detailed geometrical parameters are presented in Table I.

TABLE I
Dimensions of the Proposed Antenna Element (Units: mm)

Parameters	w_{p1}	w_{p2}	w_{p3}	w_{d1}	w_{d2}	w_{t1}	w_{t2}	w_{t4}
Values	1.96	1.64	0.64	0.15	0.21	0.12	0.12	0.12
Parameters	w_{t5}	w_{t6}	w_{t7}	w_{t8}	w_{r1}	w_{r2}	w_{r3}	w_{r4}
Values	0.45	0.24	0.14	0.16	1.25	0.74	0.3	1
Parameters	w_{r5}	w_{s1}	w_{s2}	l_{p1}	l_{t1}	l_{t2}	l_{t3}	l_{t4}
Values	1.5	0.22	0.12	1.96	0.82	1.39	0.97	0.25
Parameters	l_{t6}	l_{t7}	l_{t8}	l_{s1}	l_{s2}	c_{t1}		
Values	1.84	2.09	1.63	2.3	0.95	0.72		

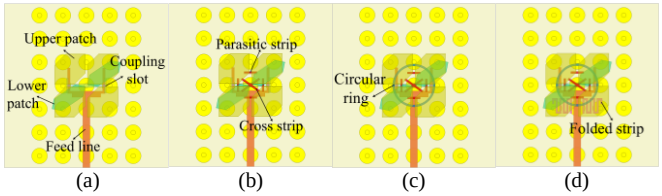

Fig. 3. Top views of the antennas. (a) Ant I. (b) Ant II. (c) Ant III. (d) Ant IV.

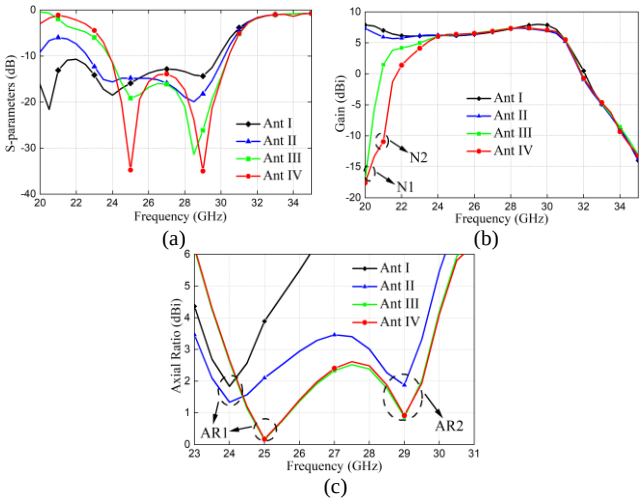

Fig. 4. Simulated performances of the Ants I–IV. (a) Reflection coefficient. (b) Realized gain. (c) ARBW.

B. Design Mechanism of CP Antenna

To investigate the operating mechanism of the CP antenna, two reference antennas, denoted as Ant I and Ant II, are designed and compared, as illustrated in Fig. 3. Fig. 4 presents the corresponding simulation results. It can be seen from Fig. 4(c) that Ant I exhibits a relatively narrow ARBW. To address this issue, cross and parasitic strips are added to Ant II, introducing a new axial ratio minimum, denoted as AR2. As a result, Ant II achieves a significant improvement in ARBW.

For clearer insight into the underlying mechanism of circular polarization, Fig. 5 depicts the surface current distribution on the cross strip. As depicted, the surface current at phase angles of 0 °, 90 °, 180 °, and 270 ° rotates consistently in the clockwise direction. Thus, the proposed design supports left-handed circularly polarized (LHCP) radiation.

C. Operating Principle of Filtering Antenna

1) Analysis of Upper Stopband Suppression

The simulated results of Ants I–IV are shown in Fig. 4. From Fig. 4(b), it can be seen that Ant I achieves good out-of-

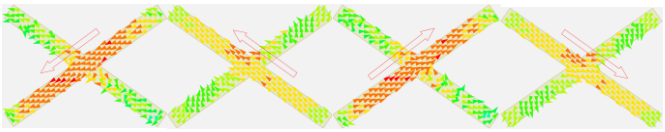

(a) (b) (c) (d)

Fig. 5. Simulated current distribution on the cross strip at f_{AR2} for phases of (a) 0 °, (b) 90 °, (c) 180 °, and (d) 270 °.

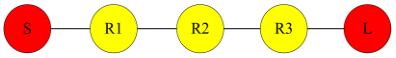

Fig. 6. Coupling topology of the third-order filter. (R1, R2, R3, S, and L denote the feeding network, the coupling slot, the antenna unit, the source, and the load, respectively.)

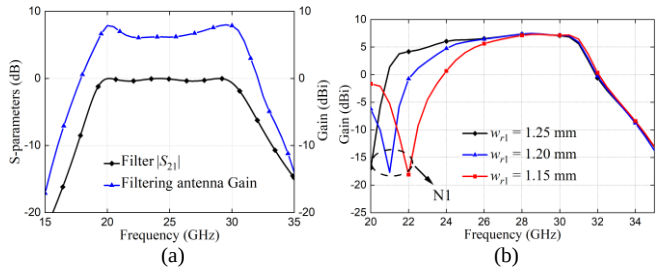

(a) (b)

Fig. 7. (a) $|S_{21}|$ of the third-order filter and realizable gain of the filtering antenna. (b) Simulated gains of Ant III with variable w_{r1}.

band suppression without parasitic structures. This effect is likely due to the antenna unit, coupling slot, and feeding network exhibiting similar resonant frequencies, resulting in the formation of a third-order filter. To facilitate a clearer explanation, Fig. 6 depicts the coupling topology of the filtering antenna. Furthermore, Ant I exhibits a –10 dB IBW of 41.3% at a center frequency of 24.7 GHz. Based on these design specifications, the normalized coupling matrix (M_{ij}) of the third-order filter can be expressed as follows [26]:

$$M_{S1} = M_{3L} = 0.82 \quad M_{12} = M_{23} = 0.78 \tag{1}$$

Subsequently, the frequency response of the third-order filter can be readily obtained based on the filter synthesis theory [29]. To facilitate comparison, the gain of Ant I and the transmission coefficient $|S_{21}|$ of the third-order filter are presented in Fig. 7(a). Clearly, the two curves show similar trends, further confirming the validity of the preceding analysis. Therefore, Ant I inherently offers high-frequency filtering, without requiring additional parasitic structures for upper stopband suppression.

2) Analysis of Lower Stopband Suppression

To enhance the lower stopband suppression of Ant III, a circular ring is introduced. As illustrated in Fig. 4(b), a radiation null, N1, appears at around 20 GHz, resulting in an out-of-band suppression exceeding 20 dB in the lower stopband. To facilitate the explanation of the radiation null mechanism, Fig. 8 depicts the surface current distribution of the upper GSPA and the circular ring at f_{N1} = 20 GHz. As observed, at f_{N1}, the energy is mainly confined to the circular ring, with little coupling to the radiating element. Therefore, Ant III achieves good suppression in the lower stopband.

Fig. 7(b) presents the variation of the realized gain of Ant III with respect to different values of w_{r1}. It can be observed that as w_{r1} decreases, the position of N1 gradually shifts from 20 GHz to 22 GHz. This indicates that the suppression level in

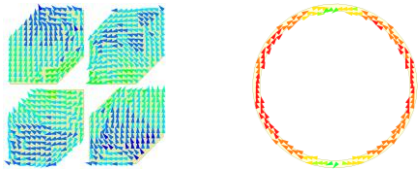

(a) (b)

Fig. 8. Simulated surface current distribution. (a) GSPA. (b) Circular ring.

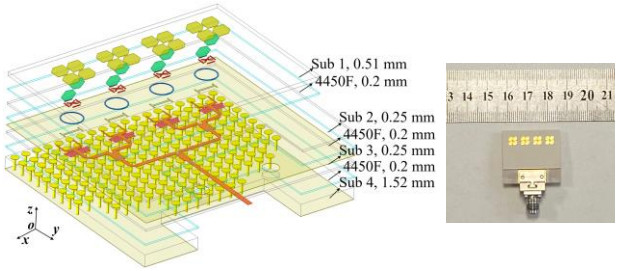

(a) (b)

Fig. 9. (a) Exploded view of the proposed 1 × 4 CP filtering antenna array. (b) Prototype of the proposed antenna array.

the lower stopband can be effectively controlled by adjusting the radius of the circular ring. Since the circular ring operates at a full-wavelength resonance in the proposed design, the relationship between the ring radius w_{r1} and the radiation null frequency f_{N1} can be expressed as follows:

$$f_{N1} = \frac{c}{2\pi w_{r1}\sqrt{\varepsilon_r}} \tag{7}$$

where c denotes the speed of light in vacuum, and ε_r represents the effective dielectric constant.

Although Ant III achieves good out-of-band suppression, its gain roll-off rate can be further improved. To address this issue, two folded strips are incorporated into Ant III, forming Ant IV. From Fig. 4(b), Ant IV provides at least a 10 dB improvement in out-of-band suppression at f_{N2} = 21 GHz compared with Ant III. Based on transmission line theory [30], resonance occurs when the electrical length of the folded strip is exactly equal to half a wavelength. Under this condition, the resonant frequency can be expressed as follows:

$$f_{N2} = \frac{c}{2L_{st}\sqrt{\varepsilon_r}} \tag{8}$$

where L_{st} = ($5l_{t3}$ + $5w_{t4}$ + l_{t4}) denotes the total length of the folded strip.

As illustrated in Fig. 4, Ant IV achieves a -10 dB IBW of 24% (23.9–30.4 GHz) and a 3 dB ARBW of 21.7% (23.9–29.75 GHz), both fully covering the entire 5G MMW band. Meanwhile, out-of-band suppression of the antenna exceeds 20 dB in the stopbands.

III. CP Filtering Antenna Array

A. Configuration Antenna Array Configuration

To validate the effectiveness of the antenna element design methodology, a 1 × 4 CP filtering GSPA array is designed, with its geometry depicted in Fig. 9(a). The antenna array is primarily composed of four layers of Rogers 3003 and three layers of Rogers 4450F substrates. The thickness of each substrate layer is identical to that of the antenna element. In addition, the spacing

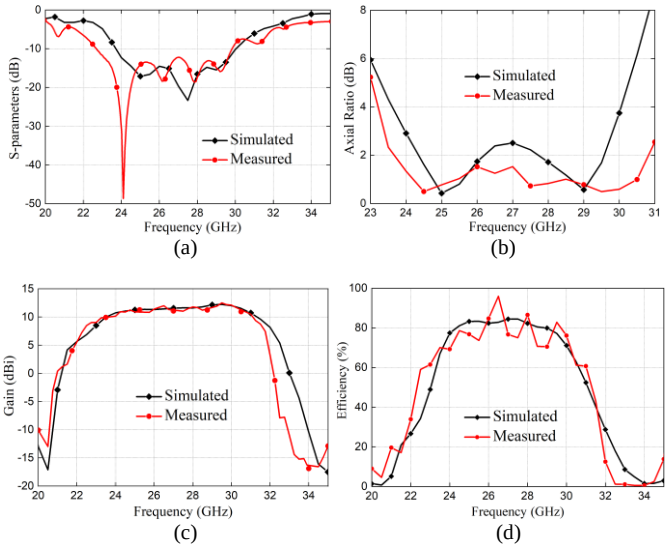

Fig. 10. Simulated and measured results of the CP filtering antenna array. (a) $|S_{11}|$. (b) Axial Ratio. (c) Realized Gain. (d) Radiation efficiency.

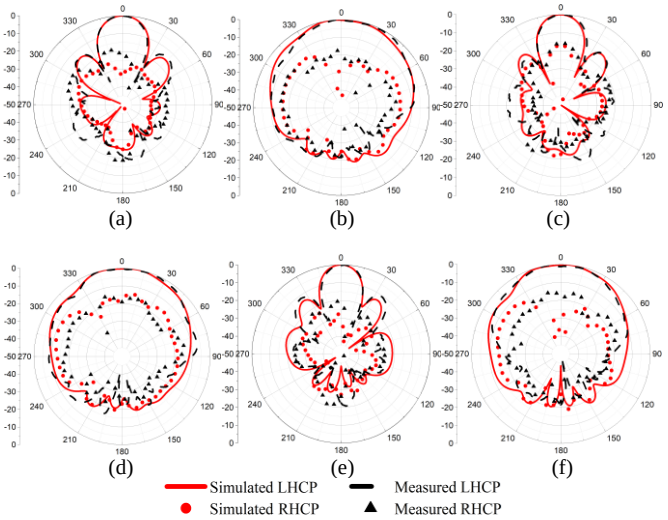

Fig. 11. Simulated and measured normalized radiation patterns of the CP filtering antenna array. (a) 25 GHz in the *xoz* plane. (b) 25 GHz in the *yoz* plane. (c) 27 GHz in the *xoz* plane. (d) 27 GHz in the *yoz* plane. (e) 29 GHz in the *xoz* plane. (f) 29 GHz in the *yoz* plane.

between adjacent antenna elements is 0.55 λ_0 at 27 GHz.

B. Experimental Results

For experimental validation, a 1 × 4 CP filtering antenna array is fabricated, as illustrated in Fig. 9(b). The simulated and measured S-parameters, ARBW, gain, and radiation efficiency are presented in Fig. 10. As depicted, the measured −10 dB IBW is 23.3%, ranging from 23.71 to 30 GHz, whereas the simulated −10 dB IBW is 26.1%, ranging from 22.74 to 29.8 GHz. It should be noted that some fluctuations and deviations are observed in the measured S-parameters, which may be attributed to fabrication tolerances, connector effects, and measurement errors. Similar behavior has also been observed in the filtering antenna reported in [9]. Meanwhile, the measured 3 dB ARBW is 27.8% (23.5–31 GHz), slightly wider than the simulated value of 21.7% (23.97–29.82 GHz). From Fig. 10(c), the measured peak gain is 12.5 dBi, whereas the simulated value is 12.25 dBi. In addition, the measured out-of-band attenuation exceeds 25 dB and 22 dB in the upper and lower stopbands, respectively. Across the operating bandwidth, the measured radiation efficiency exceeds 70%, reaching a peak value of 95%. Additionally, the radiation efficiency decreases rapidly to below 10% in both the upper and lower stopbands, further demonstrating the high out-of-band suppression capability of the proposed design.

Fig. 11 presents the simulated and measured normalized radiation patterns of the antenna array at 25, 27, and 29 GHz, respectively. As illustrated, the radiation patterns of the antenna remain stable and symmetric across the entire operating bandwidth. Besides, the measured sidelobe levels in the *xoz* plane are below −11 dB.

TABLE II
COMPARISON OF THE PROPOSED CP FILTERING ANTENNA WITH PREVIOUSLY REPORTED DESIGNS

Ref.	f_0 (GHz)	Pol.	Element size ($\lambda_0 \times \lambda_0$)	IBW (%)	ARBW (%)	Gain (dBi)	SL (dB)
[14]	7	LP	0.77 ×0.77	17.6%	N.A.	8	17
[27]	10	LP	0.62 ×0.62	4%	N.A.	9.1	11.6
[28]	4.43	LP	1.2 ×1.2	6.1%	N.A.	6.5	27
[22]	31	LP	N.A.	14.2%	N.A.	9.6	19.6
[29]	26	LP	0.55 ×0.53	12.7%	N.A.	16.8	31
[9]	30.5	CP	0.7 ×0.7	19.3%	16.4%	13	14
[10]	25.3	CP	0.51 ×0.51	14.1%	10.9%	6	35
[11]	28	CP	0.77 ×0.77	14.4%	15.3%	23.9	39
This work	**27**	**CP**	**0.37 ×0.37**	**23.3%**	**27.8%**	**12.5**	**22**

MED: Magneto-electric dipole. N.A.: Not applicable. SL: Suppression Level

C. Comparison and Discussion

The performance of the proposed work in comparison with other similar filtering antennas is summarized in Table II. As shown, although the designs reported in [14], [27], and [28] demonstrate superior out-of-band suppression, their operational frequency is confined to the low-frequency range. To address the above issues, several MMW wideband filtering antennas have been proposed [22], [29]. Nevertheless, these designs are limited to LP radiation. To date, only a few MMW CP filtering antennas have been demonstrated [9]–[11]; however, their IBW or ARBW do not fully cover the entire 5G MMW band. In addition, the aperture sizes of the majority of the aforementioned antennas exceed 0.5 λ_0 × 0.5 λ_0, which may limit their applicability in MMW antenna arrays [16]. Through comparative analysis, the proposed design is shown to simultaneously achieve wide IBW, wide ARBW, compact size, and good out-of-band suppression. Overall, the proposed CP filtering antenna array shows potential for MMW applications.

IV. CONCLUSION

In this paper, a MMW CP filtering GSPA is proposed based on the SIGW technique. The operating mechanism of the antenna is analyzed. To validate the effectiveness of the proposed design approach, a 1 × 4 CP filtering antenna array was designed and fabricated. Measurement results indicate that an IBW of 23.3%, an ARBW of 27.8%, and a peak gain of 12.5 dBi are achieved. In addition, out-of-band suppression exceeding 22 dB is achieved in both the upper and lower stopbands. Therefore, the proposed design is promising for applications in the 5G MMW band.

REFERENCES

[1] W. Hong *et al.*, "The role of millimeter-wave technologies in 5G/6G wireless communications," *IEEE J. Microw.*, vol. 1, no. 1, pp. 101-122, Jan. 2021.

[2] J. F. Harvey, M. B. Steer, and T. S. Rappaport, "Exploiting high millimeter wave bands for military communications, applications, and design," *IEEE Access*, vol. 7, pp. 52350-52359, Apr. 2019.

[3] D. Zhao, F. Lin, H. Sun, and X. Y. Zhang, "A miniaturized dual-band SIW filtering antenna with improved out-of-band suppression," *IEEE Trans. Antennas Propag.*, vol. 70, no. 1, pp. 126-134, Jan. 2022.

[4] Y. Zhang, T. Liu, L. Feng, X. Zhang, and S.-W. Wong, "A coupling matrix synthesis design for filtering antenna with good out-of-band suppression," *IEEE Antennas Wireless Propag. Lett.*, vol. 22, no. 7, pp. 1582-1586, Jul. 2023.

[5] K.-R. Xiang, F.-C. Chen, Q. Tan, and Q.-X. Chu, "High-selectivity filtering patch antennas based on multipath coupling structures," *IEEE Trans. Microw. Theory Techn.*, vol. 69, no. 4, pp. 2201-2210, Apr. 2021.

[6] G. Cheng, J. Zhou, B. Huang, L. Yang, and Z. Huang, "Compact low-profile wideband filtering antenna without additional filtering structure," *IEEE Antennas Wireless Propag. Lett.*, vol. 22, no. 10, pp. 2477-2481, Oct. 2023.

[7] Y. Li, Z. Zhao, Z. Tang, and Y. Yin, "Differentially fed, dual-band dual-polarized filtering antenna with high selectivity for 5G sub-6 ghz base station applications," *IEEE Trans. Antennas Propag.*, vol. 68, no. 4, pp. 3231-3236, Apr. 2020.

[8] D. Yang, H. Zhai, C. Guo, and H. Li, "A compact single-layer wideband microstrip antenna with filtering performance," *IEEE Antennas Wireless Propag. Lett.*, vol. 19, no. 5, pp. 801-805, May 2020.

[9] Z. Xiao, Y. Cao, W. Che, and Q. Xue, "Millimeter-wave filtering circularly polarized antenna using hybrid radiation modes for satellite applications," *IEEE Trans. Antennas Propag.*, vol. 72, no. 10, pp. 7584-7593, Aug. 2024.

[10] Y. Yang *et al.*, "A low-profile wideband circularly polarized filtering antenna based on SIW cavity TE110 mode for millimeter-wave applications," *IEEE Antennas Wireless Propag. Lett.*, vol. 24, no. 8, pp. 2352-2356, Aug. 2025.

[11] W. Wang *et al.*, "Millimeter-wave compact wideband high-gain 8 ×8 cp filtenna array with densified 16-way SIW feeding network," *IEEE Trans. Antennas Propag.*, vol. 72, no. 6, pp. 5283-5288, Jun. 2024.

[12] V. Shanmugam Bhaskar and E. L. Tan, "Same-sense circularly polarized grid-slotted patch antenna with wide axial ratio bandwidth," *IEEE Trans. Antennas Propag.*, vol. 70, no. 2, pp. 1494-1498, Feb. 2022.

[13] A. Azari, A. Skrivervik, and H. Aliakbarian, "A mmwave low complexity and low-cost super wideband dual-polarized aperture coupled antenna for 5G applications," *IEEE Access*, vol. 12, pp. 85601-85607, Jun. 2024.

[14] W. Yang *et al.*, "Novel filtering method based on metasurface antenna and its application for wideband high-gain filtering antenna with low profile," *IEEE Trans. Antennas Propag.*, vol. 67, no. 3, pp. 1535-1544, Mar. 2019.

[15] J. Guo *et al.*, "Design of a circuit-free filtering metasurface antenna using characteristic mode analysis," *IEEE Trans. Antennas Propag.*, vol. 70, no. 12, pp. 12322-12327, Dec. 2022.

[16] W. E. I. Liu, Z. N. Chen, X. Qing, J. Shi, and F. H. Lin, "Miniaturized wideband metasurface antennas," *IEEE Trans. Antennas Propag.*, vol. 65, no. 12, pp. 7345-7349, Dec. 2017.

[17] D. Chen, W. Yang, W. Che, and Q. Xue, "Miniaturized wideband metasurface antennas using cross-layer capacitive loading," *IEEE Antennas Wireless Propag. Lett.*, vol. 21, no. 1, pp. 19-23, Sep. 2022.

[18] Z. Wu *et al.*, "Miniaturized wideband metasurface antenna using fully multiplexed structure," *IEEE Antennas Wireless Propag. Lett.*, vol. 24, no. 7, pp. 1784-1788, Jul. 2025.

[19] S. J. Yang, Y. M. Pan, L.-Y. Shi, and X. Y. Zhang, "Millimeter-wave dual-polarized filtering antenna for 5G application," *IEEE Trans. Antennas Propag.*, vol. 68, no. 7, pp. 5114-5121, Jul. 2020.

[20] X. Xiong, W. Xue, J. Qi, W. Shang, and W. Li, "Miniaturized wideband metasurface antenna with filtering performance for 5G application," *IEEE Antennas Wireless Propag. Lett.*, vol. 24, no. 1, pp. 3-7, Jan. 2025.

[21] J. Zhang, X. Zhang, D. Shen, and A. A. Kishk, "Packaged microstrip line: A new quasi-tem line for microwave and millimeter-wave applications," *IEEE Trans. Microw. Theory Techn.*, vol. 65, no. 3, pp. 707-719, Mar. 2017.

[22] L. Wang *et al.*, "A high-gain controllable radiation nulls SIGW filtering antenna with improved selectivity for 5G millimeter-wave applications," *IEEE Antennas Wireless Propag. Lett.*, vol. 23, no. 12, pp. 4328-4332, Dec. 2024.

[23] M. Hui, L. Li, P. Jiang, M. Zhang, and Y. Wang, "Integrated substrate gap waveguide millimetre-wave filtering antenna with four controllable radiation nulls," *The Journal of Engineering*, vol. 2024, no. 9, Sep. 2024.

[24] X. Zhong *et al.*, "Circularly polarized filtering antenna based on integrated substrate gap waveguide," in *IEEE MTT-S Int. Wireless Symp. (IWS)*, 2021, pp. 1-3.

[25] P. S. Kildal, A. U. Zaman, E. Rajo-Iglesias, E. Alfonso, and A. Valero-Nogueira, "Design and experimental verification of ridge gap waveguide in bed of nails for parallel-plate mode suppression," *IET Microw., Antennas Propag.*, vol. 5, no. 3, pp. 262–270, Feb. 2011.

[26] R. J. Cameron, C. M. Kudsia, and R. R. Mansour, *Microwave Filters for Communication Systems: Fundamentals, Design, and Applications*. Hoboken, NJ, USA: Wiley, 2007.

[27] K. R. Xiang, F. C. Chen, and Q. X. Chu, "High selectivity and high gain x-band waveguide filtering antenna based on triple-mode resonator," *IEEE Trans. Antennas Propag.*, vol. 69, no. 10, pp. 6953-6958, Apr. 2021.

[28] P. K. Li *et al.*, "Codesigned high-efficiency single-layered substrate integrated waveguide filtering antenna with a controllable radiation null," *IEEE Antennas Wireless Propag. Lett.*, vol. 17, no. 2, pp. 295-298, Dec. 2018.

[29] B. Feng, J. Chen, K. L. Chung, L. Wang, and Y. Li, "Dual-polarized filtering magneto-electric dipole antenna arrays with high radiation-suppression index for 5G new radio n258 operations," *IEEE Trans. Antennas Propag.*, vol. 70, no. 4, pp. 3058-3063, Apr. 2022.